Flow simulation of a two dimensional rectangular supersonic convergent divergent nozzle

E. M. S. Ekanayake[1]   J. A. Gear[2]   Y. Ding[3]

Abstract

A two dimensional convergent-divergent nozzle with a rectangular cross section is modelled under ambient conditions experienced by a supersonic jet engine at cruising altitude. Instability due to shock wave formation at the divergent section of the nozzle and Mach shocks downstream of the jet plume region are investigated. The nozzle:pressure ratio significantly affects the shock location. Nozzle exit to throat area ratios of 1.5 and 1.66 with divergent angles of $2.801°$ and $3.89°$ are investigated numerically with the shear stress transport model of ANSYS-CFX. The numerical study is carried out to understand the influence of the nozzle geometry and pressure ratio on flow properties downstream of the nozzle and the external jet plume region.

Contents

1 Introduction

The need for new supersonic commercial aircraft and military jets of higher speeds with improved thrust and advanced propulsion capabilities is a growing future interest in the aerospace industry. The shape of the nozzle is the key to the expansion process, it plays a vital part towards minimising thrust loss by expanding the exhaust gases exiting the nozzle to their maximum potential. Supersonic convergent-divergent (CD) nozzles are used not only on military jets but also in rocket nozzles and significantly on current high speed missiles.

When the gas exits the nozzle at supersonic speeds, it undergoes several flow phenomena depending on the nozzle:pressure ratio (the ratio of inlet to outlet pressure, NPR). Identification of the flow separation within nozzles is important as separation decreases flow speed hence increasing drag.

Nozzle flow separation is highly dependent on local turbulence levels, Reynolds number, viscous wall effects and the pressure ratio. Total pressure loss, unsteadiness, instability, loss of flow control performance are some of the drawbacks experienced by an internal flow (nozzle/diffuser) [1, 2]. But enhanced mixing efficiency and increased turbulence level have given experimentalists

some potential applications for nozzle flows under low pressure ratios. Some experimental and computational simulations have been done for gases emerging through a CD nozzle under low pressure ratios and free stream Mach number 0.1. These investigations were mainly focused on the mixing enhancement for potential applications towards fuel injection and thermal signature reductions in jet engine fuel systems [3, 4, 5]. Other computational studies analysed the effects downstream of pressure ratio ($\leqslant 3.0$), aspect ratio, and Mach number for nozzles with exit to throat area ratio (NAR) 1.5 [6, 7].

Two primary wave structures known as the overexpanded and underexpanded conditions cause Mach diamond flow patterns to form. These Mach disks are enclosed by a layer known as the free jet boundary which gradually dissipates away due to viscous damping.

Evidence from previous experiments proves a non-circular nozzle shape expands the gas faster than a circularly contoured nozzle wall. We discuss nozzle:pressure ratios varying from very low to high, and also the effect of geometry variation. Two test cases were carried out for supersonic jet nozzles, operating at real atmospheric conditions, one during high altitude (228 K) and the other at sea-level (290 K). A two dimensional, axi-symmetric, CD rectangular nozzle was modelled numerically using the shear stress transport model in ANSYS-CFX.

2   Instability and nozzle flow separation

When a shock wave interacts with a boundary layer, many diverse types of flow phenomena occur: flow separation, unsteadiness, complicated mixing, turbulence, shock induced boundary layer separation, and so on [1]. The instability initiated by the shock wave boundary layer interaction of a supersonic CD nozzle plays a crucial part where the exhaust gas losses its kinetic energy and decelerates thereby decreasing thrust.

When the static pressure is increased, an adverse pressure gradient can cause
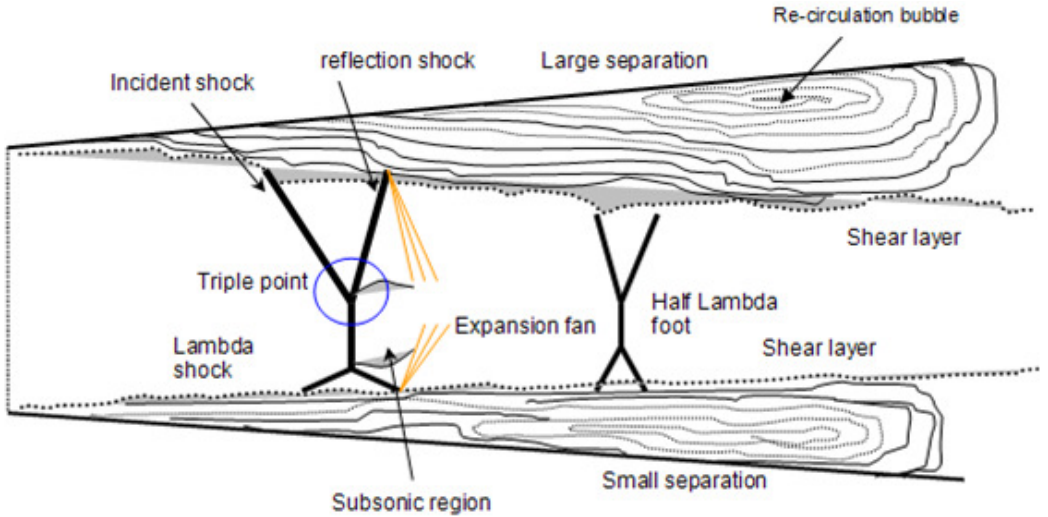
FIGURE 1: Lambda foot shock wave.

the boundary layer to detach from the nozzle wall surface. This increase in static pressure, which contributes to increased potential energy of the gas, thereby decreases the kinetic energy of the flow. The inner layer of the boundary which is relatively slow is significantly affected by this increasing static pressure, large enough to bring the velocity to zero or become reversed. The phenomena of flow reversal causes the flow to separate from the surface creating a circulation bubble (Figure 1).

Instabilities commence as shock induced flow separation, as the pressure ratio increases the flow becomes overexpanded, uniform and finally under-expanded. At low nozzle:pressure ratios flow separation undergoes several critical transitions starting from symmetric to asymmetric and finally becomes symmetric before exiting the nozzle. Due to shock wave boundary layer interaction, the nozzle experiences strong unsteadiness initiating the flow to detach from the boundary layer. A weak form of shock is developed as a result of the asymmetric flow separation, known as Lambda shock. Incident shock and a reflection shock merge at the Mach stem, creating a

Lambda foot shock, where three waves meet at a so-called triple point (Figure 1). Downstream of the Lambda foot the flow is subsonic and a further second Lambda foot is created of half the size.

Overexpansion occurs when the pressure at the exit of the nozzle (back pressure) is less than ambient pressure causing the Normal shock wave to bend towards the jet plume. The shock wave is oblique to the wall forming a complex flow pattern exiting the nozzle as a combination of subsonic and supersonic flows. Further increasing the nozzle:pressure ratio causes the back pressure to match the ambient pressure, resulting in a smooth flow, uniform supersonic and parallel. This is the ideal design condition. Increasing the pressure further (exit pressure now greater than ambient) creates a new imbalance, where the waves at the exit of the nozzle wall turn outward as expansion waves, creating a new flow pattern where compression and expansion waves repeat downstream along the plume region (underexpanded condition).

3   Shear stress transport model and computational setup

Flows with high adverse pressure gradients, where the boundary layer detaches from the wall due to increase in static pressure in the direction of the flow, will experience several detachments along the wall surface. Analysis of separation of the nozzle down stream requires a good model with dual capabilities. Two equation models such as the k-ϵ model, k is the turbulent kinetic energy and ϵ is the turbulent dissipation, or the k-ω model, where ω is the specific rate of turbulent dissipation, fail to accurately determine flows subjected to increasing adverse pressure gradients [4]. Menter's two equation SST model is used for choked nozzle flows under adverse pressure gradient conditions. It offers optimal boundary layer simulation capabilities. Turbulent viscosity is modified to account for transport of the turbulent shear
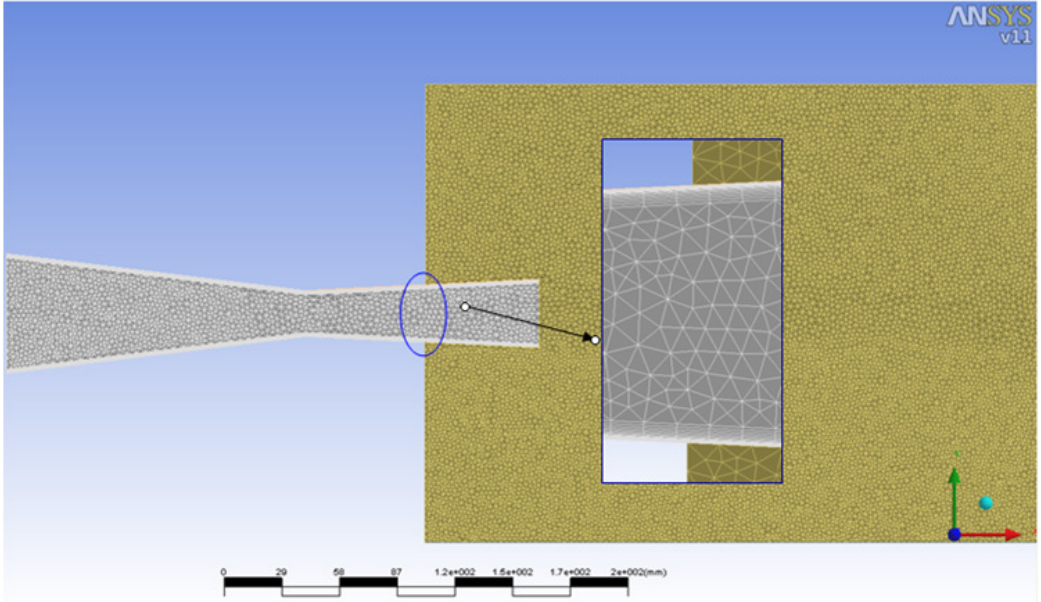
FIGURE 2: Compultional mesh setup in ANSYS CFX-mesh.

stress. The zonal formulation is a combination based on blending of proper functions of k-ε and k-ω zones without user interaction. The SST model shifts values between one and zero of the blending function, F_{sst}, to switch from near wall to bulk regions. This blending function ensures a smooth transition between k-ε and k-ω models.

The upstream length (convergent section) of the nozzle is 150 mm with convergence angle 7°. The downstream geometry (length 117 mm) is varied with nozzle:area ratios at the nozzle exit of 1.5 and 1.66, divergent angles of 2.801° and 3.89° respectively. The reference length, the nozzle height at the throat, is constant at 22.9 mm. The Reynolds number was set to 5.5×10^6 for a Y^+ value equal to one. A grid independence test was carried out for a course mesh of 32747 elements, and medium mesh of 77035 and 83932 unstructured elements with the number of inflated layers set to 35 and 45. The number

of inflated layers set to 45 with a medium mesh of 77035 elements was adequate to capture the flow characteristics inside the nozzle and jet plume. The walls were specified as adiabatic and no slip. The computational mesh was built as two body regions: the nozzle region and external plume region as shown in Figure 2. Relative pressure which is the external static pressure (ambient pressure) is 102387 Pa (1 atm). Two temperature values were used: 290 K for sea-level conditions, and 228 K approximating atmospheric conditions at 18–20 km altitude during flight. The nozzle:pressure ratio varied from 1.20 to 12 atm. The nozzle inlet temperature was set constant to 500 K. Free stream velocity entering the external flow domain was set to 250 ms^{-1} (0.727 Mach number).

4 Results and discussion

The high sensitivity of the shear stress transport model is demonstrated in the test cases carried out at low pressure ratios, see Figure 3. Some of the selected results from the large pool of simulations are summarized in Tables 1 and 2. Table 1 summarizes the Mach location (Mach.L), which is the distance to the highest Mach number measured from the throat, against nozzle:pressure ratio.

Figure 3 shows the flow downstream of the nozzle experiences asymmetric separation due to the boundary layer detachment from the wall creating a Lambda foot shock wave. The size of the flow separation region influences the size of the Lambda foot shock. In Figure 3(c) a second Lambda foot shock wave is also evident. The corresponding turbulent kinetic energy contours are shown in Figure 4. The turbulent kinetic energy is highest (100057 m^{2}s^{-2}), at nozzle:pressure ratio 1.4, see Figure 4(b). Figures 3 and 4 show that as the nozzle:pressure ratio increases the flow separation zone increases in size and moves from one wall to the opposite and back before ultimately exiting the nozzle. This transition from one wall to the other is due to the build up of turbulent kinetic energy on the opposite wall.
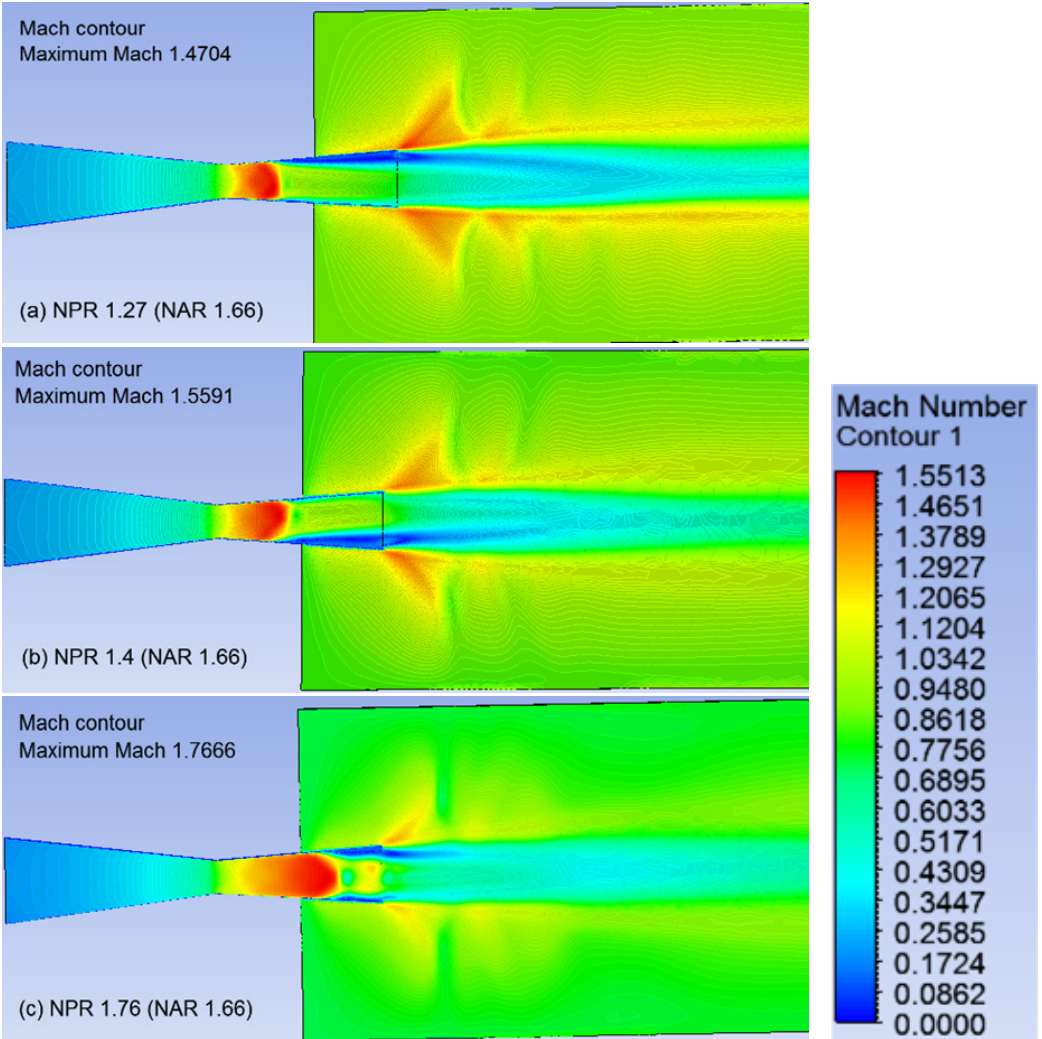
FIGURE 3: Mach number contours, at nozzle:area ratio (NAR) 1.66 at 228 K, for nozzle:pressure ratios (NPR): (a) 1.27; (b) 1.4; (c) 1.76.
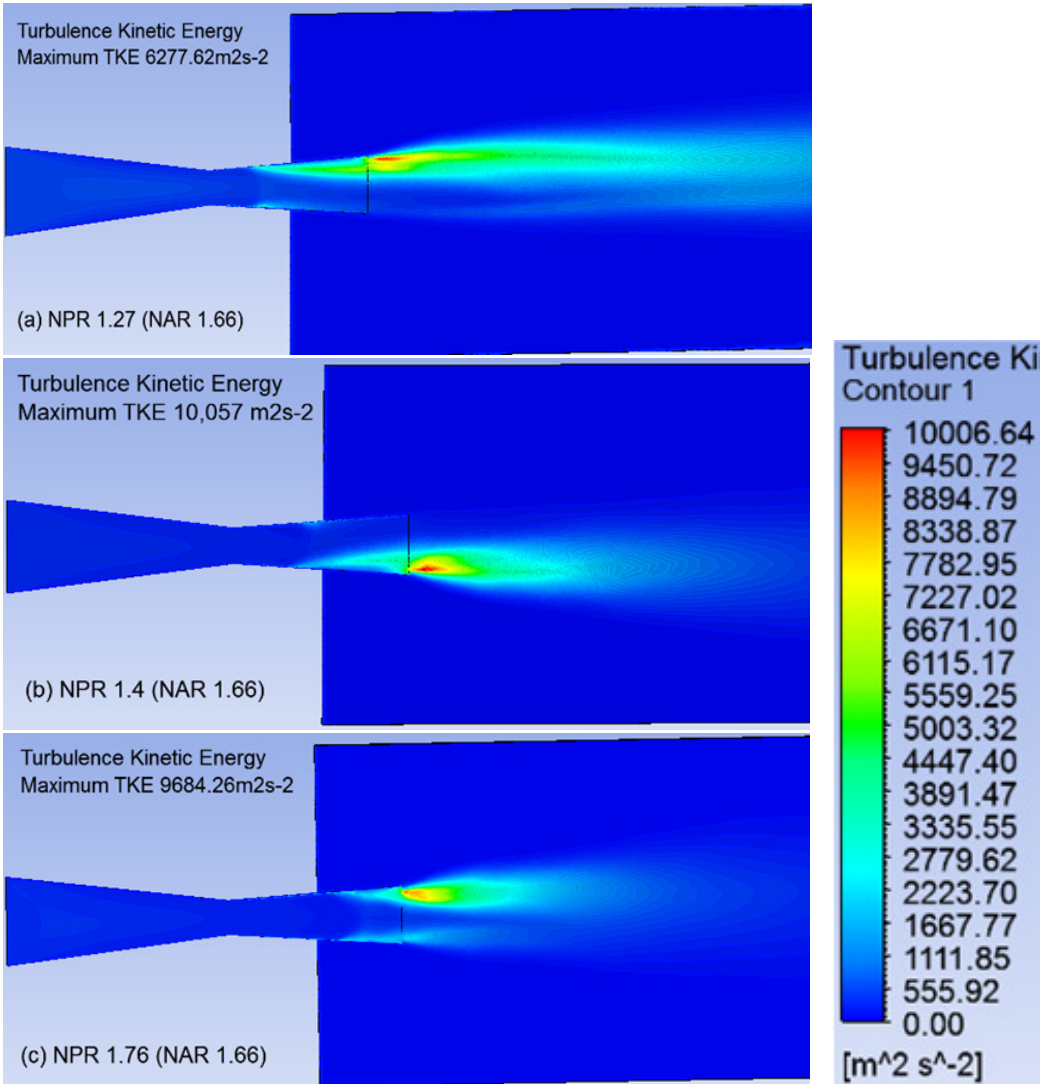
FIGURE 4: Turbulent kinetic energy contours, at nozzle:area ratio (NAR) 1.66 at 228 K, for nozzle:pressure ratios (NPR): (a) 1.27; (b) 1.4; (c) 1.76.

TABLE 1: Nozzle:pressure ratios (NPRs) at nozzle:area ratio (NAR) 1.5, for 228 K and 290 K (Mach.L: location to Highest Mach number, axial direction from the throat).

NPR	Temp = 228 K			Temp = 290 K		
	Mach No	Mach.L (m)	Separation	Mach No	Mach.L (m)	Separation
1.27	1.3778	0.02720	asymmetric	1.2262	0.01519	no separation
1.34	1.4183	0.03364	asymmetric	1.3159	0.02133	no separation
1.40	1.4640	0.04331	asymmetric	1.3473	0.02263	no separation
1.61	1.5460	0.05715	asymmetric	1.4413	0.03962	asymmetric
1.79	1.5739	0.06004	asymmetric	1.4788	0.04526	asymmetric
1.82	1.7845	0.10809	shock at exit	1.5467	0.05444	asymmetric
2.4	1.8053	0.11345	overexpanded	1.6070	0.06729	asymmetric
3.4	1.8127	0.11346	overexpanded	1.8141	0.1170	shock at exit
4.0	1.8153	0.1170	overexpanded	1.8166	0.1170	overexpanded
5.5	1.8194	0.1170	flow parallel	1.8226	0.1170	overexpanded
7.0	1.8275	0.1170	flow parallel	1.8289	0.1170	overexpanded
10.0	2.0412	0.4417	underexpanded	1.9425	0.1170	underexpanded
12.0	2.1689	0.4802	underexpanded	2.0775	0.53557	underexpanded

TABLE 2: Mach numbers for various cases: nozzle:area ratio (NAR) 1.5 and 1.66 for 228 K (altitude 20 km) and 290 K (sea-level).

NPR	NAR = 1.5		NAR = 1.66	
	228 K	290 K	228 K	290 K
1.27	1.3778	1.2262	1.4705 (symmetric)	1.3855
1.34	1.4183	1.3159	1.4733 (asymmetric)	1.3947
1.4	1.4640	1.3473	1.5591(asymmetric)	1.414
1.61	1.5460	1.4465	1.642 (asymmetric)	1.453
1.79	1.5739	1.4788	1.797 (symmetric)	1.521
1.96	1.8010	1.5228	1.899 (symmetric)	1.6405
2.4	1.8053	1.6070	1.990 (overexpanded)	1.790
3.4	1.8127	1.8141	1.998 (overexpanded)	1.8211
5.5	1.8194	1.8226	2.008 (overexpanded)	2.0083
7.0	1.8275	1.8289	2.014 (close to parallel flow)	2.009
10.0	2.0412	1.9425	2.023 (underexpanded)	2.029
12.0	2.1689	2.0775	2.053 (underexpanded)	2.057

Maximum Mach number 1.3778
(Inside nozzle)
Shock Normal to wall

(a) NPR 1.20

Maximum Mach number 1.4848
(Inside nozzle)
Asymmetric flow separation
(Lambda shock)

(b) NPR 1.47

Maximum Mach number 1.5757
(Inside nozzle)
Asymmetric flow separation
(Lambda shock)

(c) NPR 1.79

Maximum Mach number 1.7822
(Inside nozzle)
Shock at the exit

(d) NPR 1.82

Maximum Mach number 1.8407
(Inside nozzle)
Overexpanded flow
(Shock Oblique to the exit wall)

(e) NPR 2.3

Mach Number
Contour 1

2.1580
2.0381
1.9182
1.7983
1.6785
1.5586
1.4387
1.3188
1.1989
1.0790
0.9591
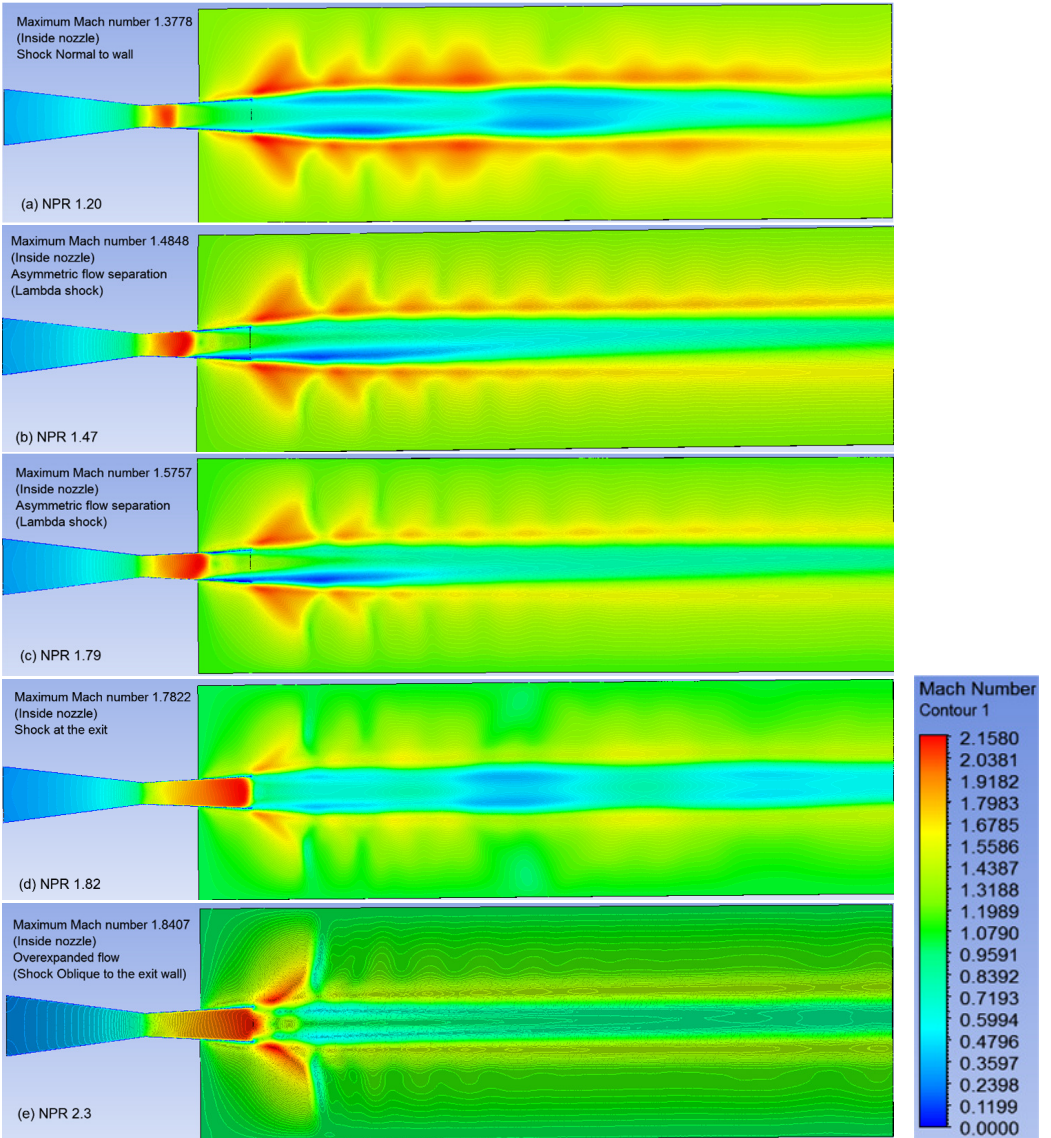0.8392
0.7193
0.5994
0.4796
0.3597
0.2398
0.1199
0.0000

FIGURE 5: Mach contours for nozzle:area ratio (NAR) 1.5, ambient temperature 228 K, and nozzle:pressure ratios (NPR): (a) 1.20; (b) 1.47; (c) 1.79; (d) 1.82; (e) 2.3.
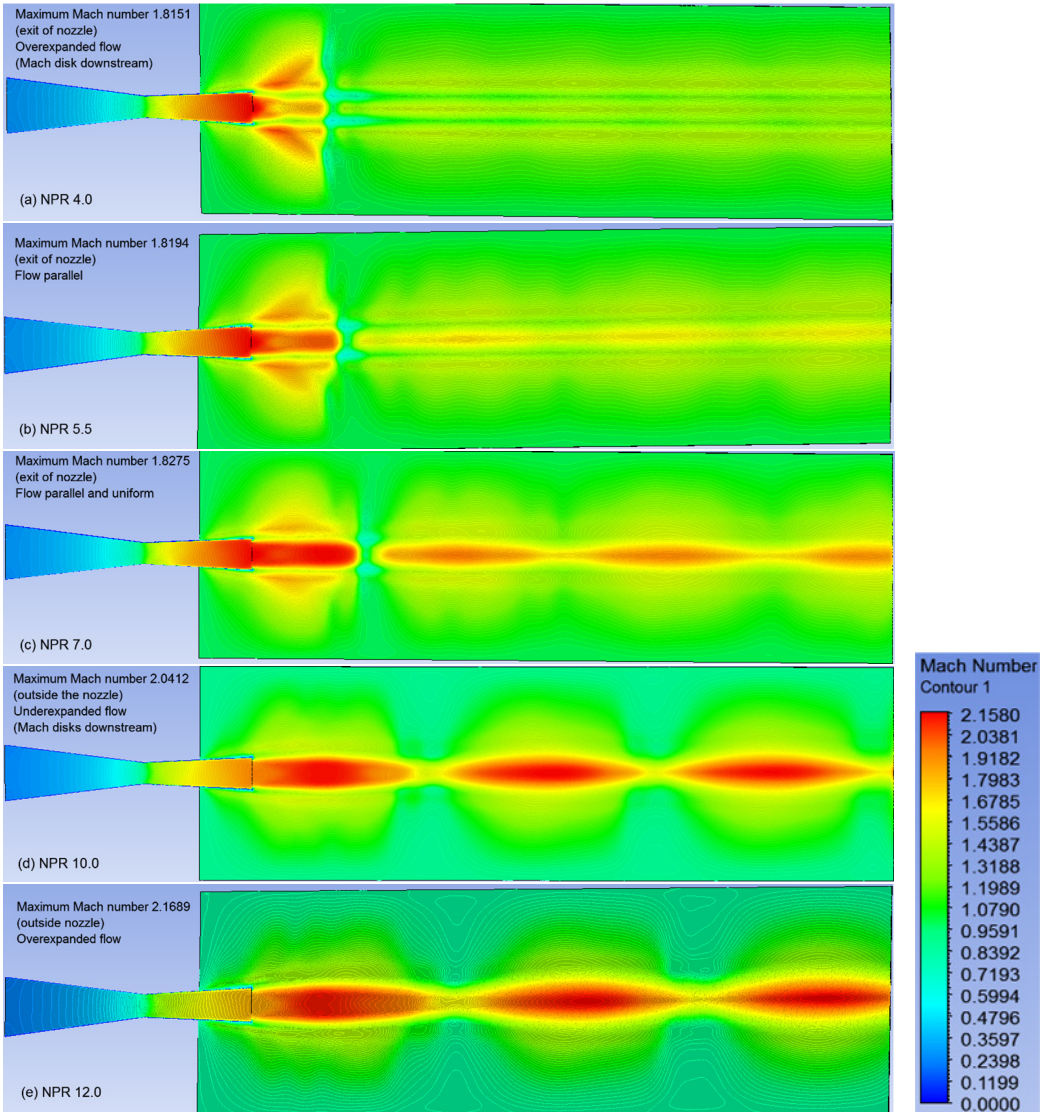
FIGURE 6: Mach contours for nozzle:area ratio (NAR) 1.5, ambient temperature 228 K, and nozzle:pressure ratios (NPR): (a) 4.0; (b) 5.5; (c) 7.0; (d) 10.0; (e) 12.0.

Figures 5 and 6, show the influence of increasing pressure ratio on the jet stream flow downstream of the nozzle and how the free stream speed $250\,\mathrm{ms}^{-1}$, influences the Mach number of the fluid exiting the nozzle.

Figure 6(c) (NPR 7.0) shows a sudden drop in Mach number from 1.8275 to 0.8. Further downstream this flow regains speed under the influence of the overexpansion and forms a pattern of shock diamonds. Table 2 shows that at low pressure ratios, the Mach number increases faster for the high area ratio case (NAR 1.66). At 228 K, the flow separation is symmetric for nozzle:pressure ratios 1.79–1.96 and uniform for high pressure ratios between about 6 and 7.0. For 290 K the symmetric flow separation starts at NPR 2.4 and lasts until 3.4 before experiencing overexpansion.

At 228 K, the location to the highest Mach number (Mach.L) remains constant at the nozzle exit (117 mm) for pressure ratios between 4.0–7.0, see Table 1, while for 290 K the location remains constant for pressure ratios between 3.4–10.0. In both cases further increase in pressure ratio causes the location of the highest mach number to move downstream of the nozzle exit.

Figures 6(c), (d) and (e) and Figure 7 compare the effect of temperature at high nozzle:pressure ratios. In Figure 7 multiple Mach diamonds form for both NPR 5.5 and 7.0 at 290 K, whereas in Figures 6(c), (d) and (e) at 228 K, only two or three Mach shocks are visible in the same length downstream of the nozzle.

References

[1] X. L. Tong and E. Luke. Turbulence Models and Heat Transfer in Nozzle Flows. AIAA 8900-356 Journal 11/2004, Vol 42, No 11, Technical Notes pages 2391–2393. doi:10.2514/1.8900 C378, C379

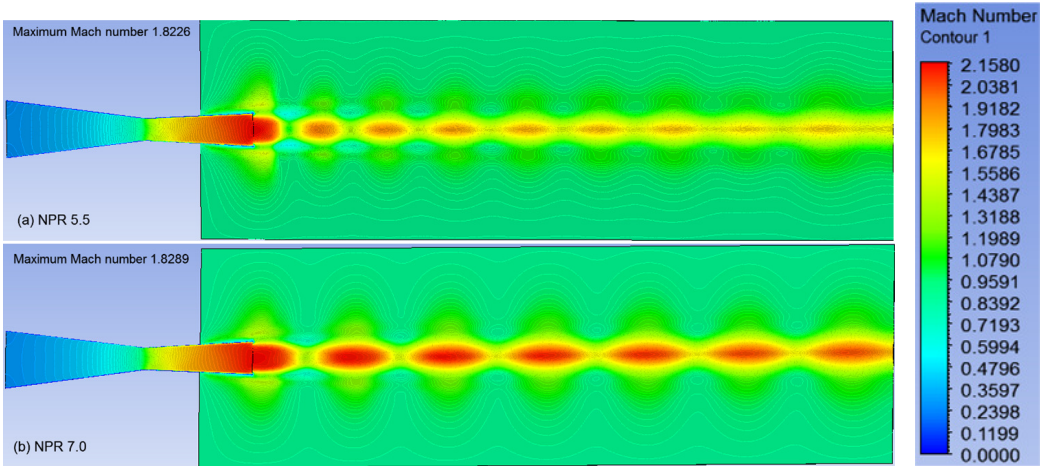[2] http://www.lmfa.ec-lyon.fr/ISAIF/Data/Invited_lectures/IL142/IL142.pdf. 8th ISAIF, Lyon, France, July 2007 C378

FIGURE 7: Mach contours for nozzle:area ratio (NAR) 1.5, for 290 K, and nozzle:pressure ratios (NPR): (a) 5.5; (b) 7.0.

[3] Q. Xiao, H. M. Tsai, D. Papamoschou and A. Johnson. Experimental and Numerical study of Jet Mixing from a Shock-Containing Nozzle. AIAA Journal of Propulsion and Power , Vol 25, No 3, 688–696, 2009. doi:10.2514/1.37022 C379

[4] Q. Xiao, H. M. Tsai and D. Papamoschou. Numerical Investigation of Supersonic Nozzle Flow Seperation. AIAA Journal, Vol 45, No 3, 532–541, 2007. doi:10.2514/1.20073 C379, C381

[5] Q. Xiao, H. M. Tsai and D. Papamoschou. Numerical study of Jet Plume Instabilty from an Overexpanded Nozzle. 45th Aerospace science Meeting and Exhibit, AIAA 2007–1319 Journal, Reno, Nevada. http://supersonic.eng.uci.edu/download/AIAA-2007-1319.pdf C379

[6] N. Menon, B. W. Skews. Rectangular underexpanded gas effects: effect of pressure ratio, aspect ratio and Mach number. Shock Waves 1, Volume 2, 26th International Symposium on Shock Waves.

doi:10.1007/978-3-540-85181-3_32 C379

[7] A. A. Khan, T. R. Shembharkar. Viscous Flow analisys in a Convergent-Divergent Nozzle. Proceedings for International Conference on Aerospace Science and Technology, 26–28 June 2008, IN-CAST 2008-004, Bangalore, India. http://nal-ir.nal.res.in/4982/01/INCAST-004.pdf C379

Author addresses

1. **E. M. S. Ekanayake**, School of Mathematical and Geospatial Sciences, RMIT University, Melbourne, Australia.

2. **J. A. Gear**, School of Mathematical and Geospatial Sciences, RMIT University, Melbourne, Australia.
   mailto:jag@rmit.edu.au

3. **Y. Ding**, School of Mathematical and Geospatial Sciences, RMIT University, Melbourne, Australia.